Figures and Legends

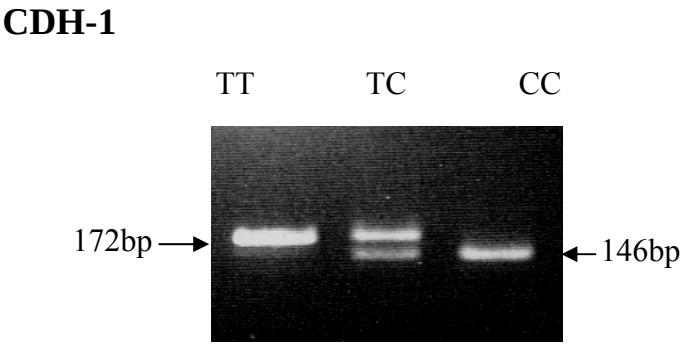

Fig. 1 The PCR products of E-cadherin gene 3'-UTR C/T polymorphism on 3% agarose gel. PCR-base restriction analysis of E-CDH gene 3'-UTR *Pml* I polymorphism shown on 3 % agarose electrophoresis. The polymorphic region was amplified by PCR which resulted in an undigestable fragment in lane 1 (172 bp), a digestable fragment in lane 3 (146-bp and 26-bp) and a heterozygote in lane 2.

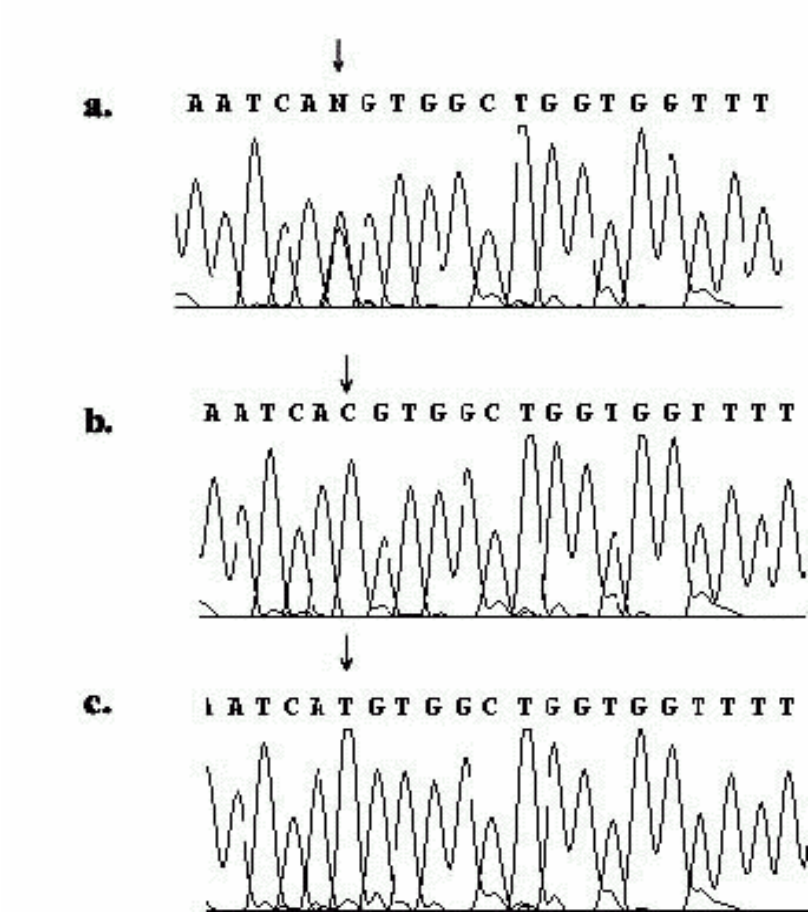

Fig. 2 The sequence of E-CDH 3'-UTR C/T polymorphism. **2a**: Sequence of PCR product with C/T heterozygote, arrow indicate the point of C/T polymorphism. **2b:** Sequence of PCR product with C/C heterozygote, arrow indicate the point of C polymorphism. **2c:** Sequence of PCR product with T/T homozygote, arrow indicate the point of T polymorphism.

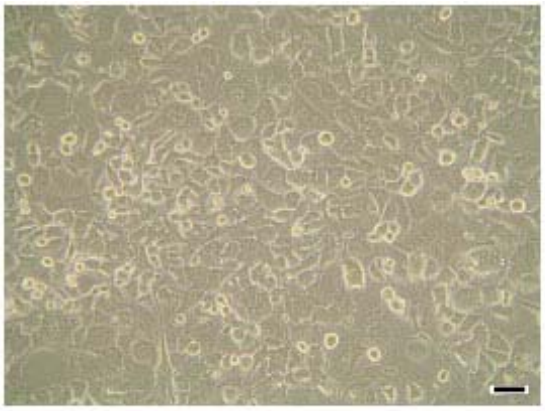

Fig. 3 N18 RGCs grew in DMEM medium. After adding hypoxanthine–aminoprerin–thymidine (HAT) medium to N18, N18 RGCs with dendritic process was seen. (Scale bar = 4 μm)

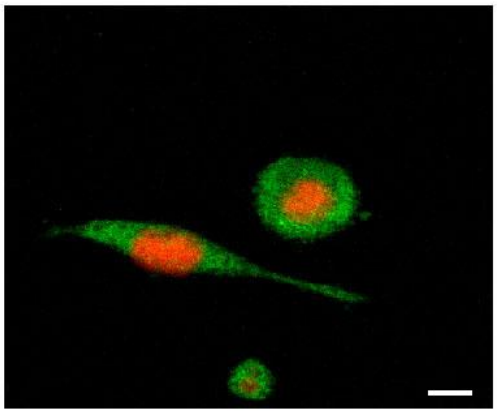

Fig. 4a RGCs stained with Thy-1 [stained with fluoresceinisothiocyanate (FITC) conjugated secondary antibody]. N18 cells were stained with Thy-1 which is specific for neural cells. The neural projections are evident. (Scale bar = 0.4 μm)

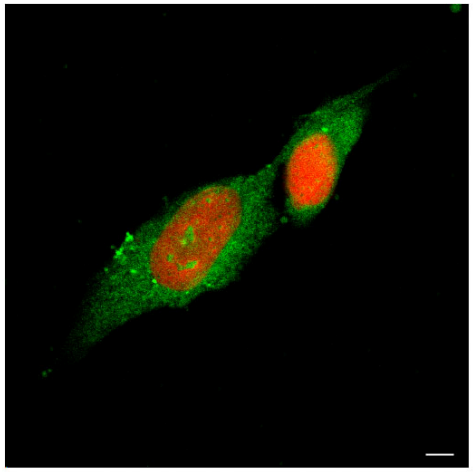

Fig. 4b N18 RGCs stained with anti-NR1. N18 RGCs stained with antibody to NMDA receptor (NR1 antibody) conjugated with FITC. (Scale bar = 0.3 μm).

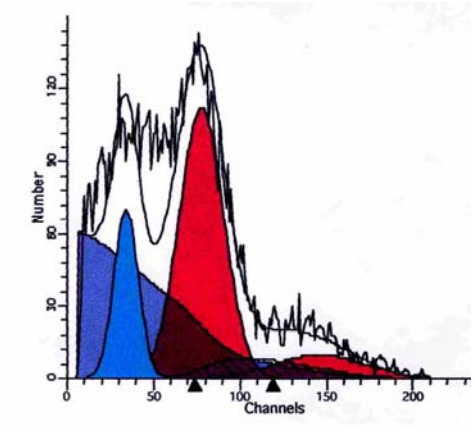

Fig. 5a NMDA induced apoptosis of RGCs at the concentration100 μM. Flow cytometry was used to detect percentage of apoptotic cells. 100 μM NMDA induced 69.9% apoptosis of N18 RGCs (red arrow head indicated cell with apoptosis).

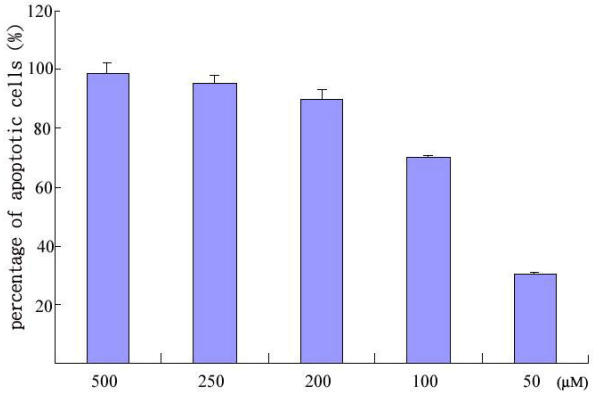

Fig. 5b Apoptosis of N18 RGCs in various concentration of NMDA. Various concentrations NMDA were added to RGCs and the apoptotic cells were detected to select appropriate concentration which can be used in this study. NMDA at the concentration 100 μM was able to induce 69.9% of apoptosis in retina ganglion cells, and was suitable to be used in this study (** p<0.001).

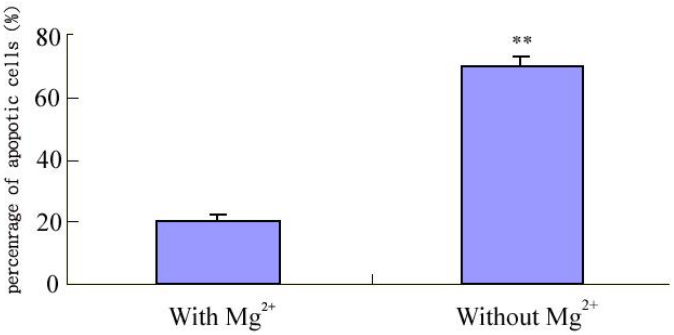

Fig. 6 NMDA induced apoptosis in solution with or without Mg^{2+}. NMDA at the concentration 100 μM induced 69.9% apoptsis of N18 RGCs in Mg^{2+} free medium. But in medium with Mg^{2+}, 100 μM NMDA just induced 20 % of apoptosis in RGCs.

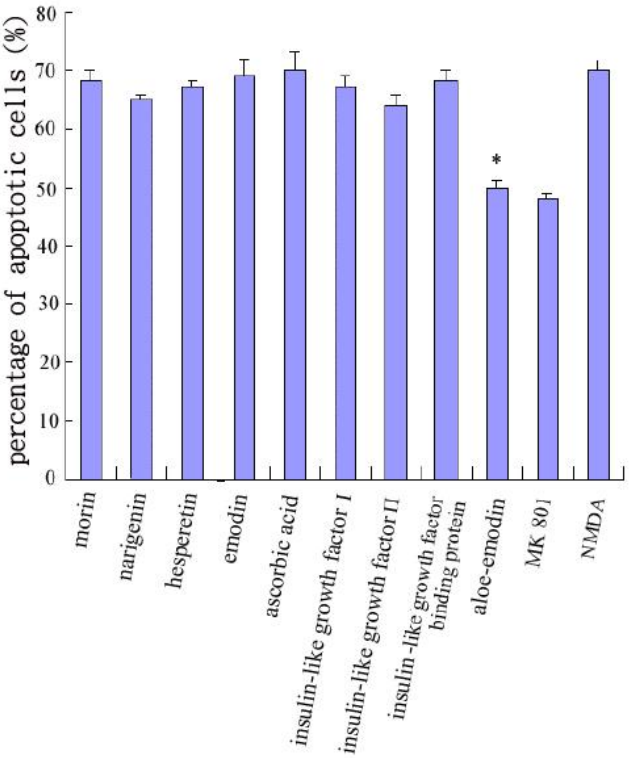

Fig. 7 The effects of neuroprotectors and polyphenols metabolites on NMDA-treated N18 RGCs. The concentrations of the aloe-emodin metaboliytes were 15 μM. The concentration of ascorbic acid was 80 M. The concentrations of IGF I, Π and IGF BP were 10 M. In the control group, only 100 M NMDA was added and it induced 69.9% apoptosis of RGCs. Aloe-emodin metabolites was the most effective among the tested agents (** $p< 0.001$). Aloe-emodin metabolits reduced the apoptosis to 50 %, which ws comparable with the effects of MK 801 which decreased apoptosis from 69.9 % to 48%.

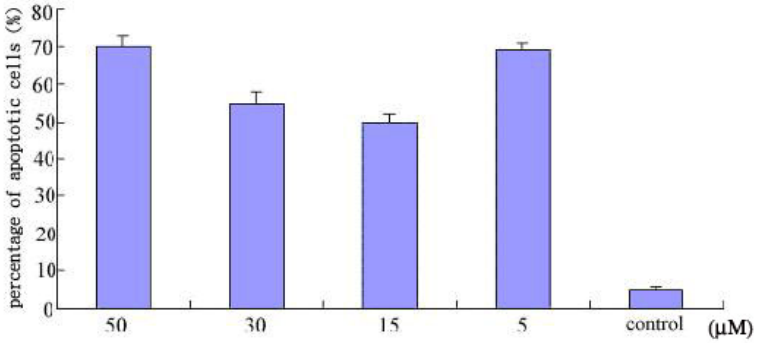

Fig. 8 The effects of different concentration of aloe-emodin metabolites on NMDA induced apoptosis in N18 RGCs**.** Aloe-emodin metabolites over then 15μM were not more effective Nevertheless, the concentrations of aloe-emodin metabolites less then 15μM were null and void on NMDA -iduced apoptosis of N18 RGCs.

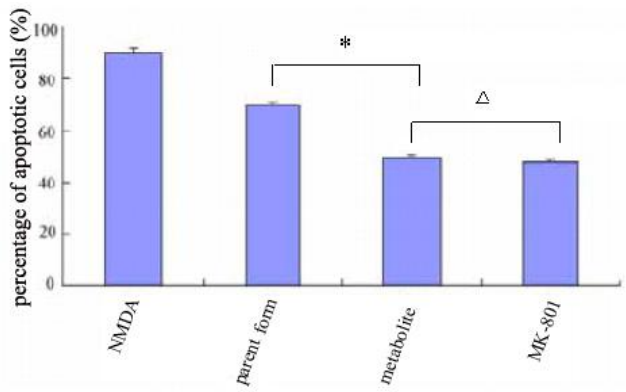

Fig. 9 The effects of parent form and metabolites of aloe-emodin on NMDA-treated N18 RGCs. At concentration of 15 μM, the parent form of aloe-emodin decreased apoptosis of RGCs from 69.9% to 62%, whereas aloe-emodin metabolites decreased apoptosis from 69.9% to 50% (* $p < 0.05$, △ $p > 0.05$).

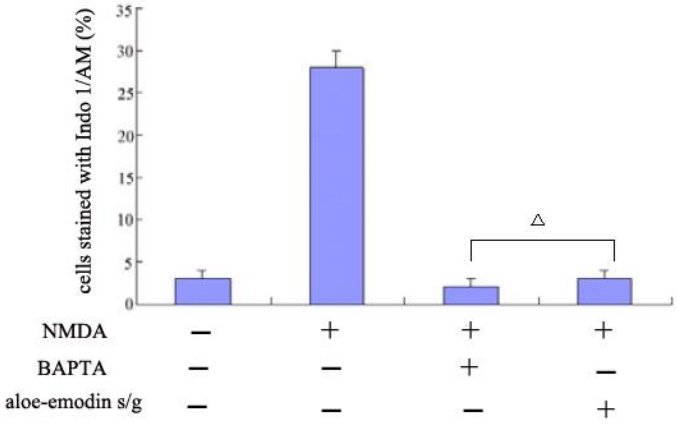

Fig. 10 The effects of aloe-emodin metabolites on Ca^{2+} concentration in NMDA-treated N18 RGCs. BAPTA (Ca^{2+} chelator) reduced cells stained with Ca^{2+} in the NMDA-treated RGCs from 27% to 4%. Aloe-emodin metabolites reduced cells stained with Ca^{2+} to 6% (△ $p > 0.05$).

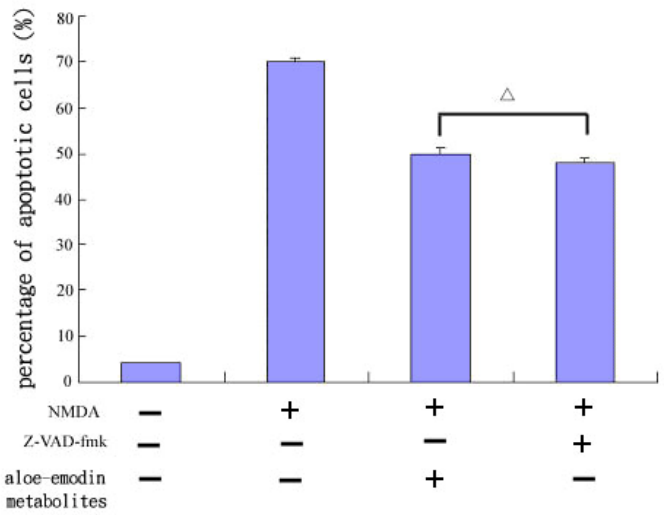

Fig. 11 The effects of aloe-emodin metabolites and caspase 3 blocker on NMDA-treated N18 RGCs. Aloe-emodin metabolites decreased the apoptosis of NMDA treated RGCs from 69.9% to 50%. The effect of aloe-emodin metabolites was comparable with that of Z-VAD-fmk (a commercial caspase-3 blocker) in increasing the cell viability. The cells apoptosis decreased from 69.9% to 48% by Z-VAD-fmk (△ $p > 0.05$).

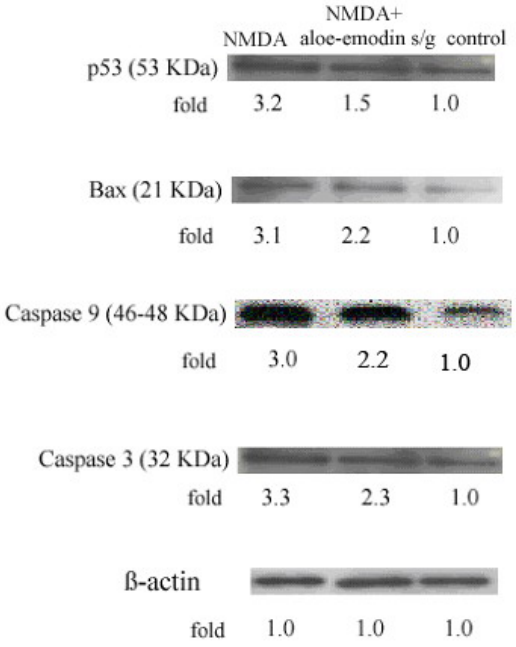

Fig. 12a-1 The effects of aloe-emodin metabolites on apoptosis pathway of NMDA-treated N18 RGCs.

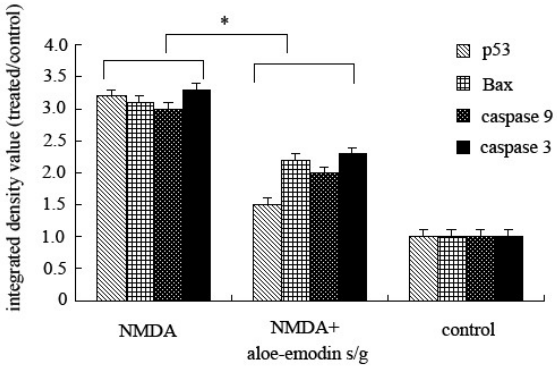

Fig. 12a-2 Western blotting analysis the effects of aloe-emodin metabolites on apoptosis pathway of NMDA-treated N18 RGCs. In the apoptosis pathway NMDA increased the expression of p53, bax, caspase 9 and caspase 3. Aloe-emodin metabolites decreased the activation of these molecules.

Fig. 12a-1 and 12a-2: Western blotting to detect molecules involved in the apoptosis of aloe-emodin metabolites and NMDA-treated N18 RGCs. All data were normalized to the control groups. In the apoptosis pathway NMDA increased the expression of p53, bax, caspase 9 and caspase 3 (line 1 of each row 1) (Fig. 14a-1). Aloe-emodin metabolites decreased the activation of these molecules (line 2 of each row 2) (Fig. 12a-1and 12a-2) (n=3) (*$p< 0.05$).

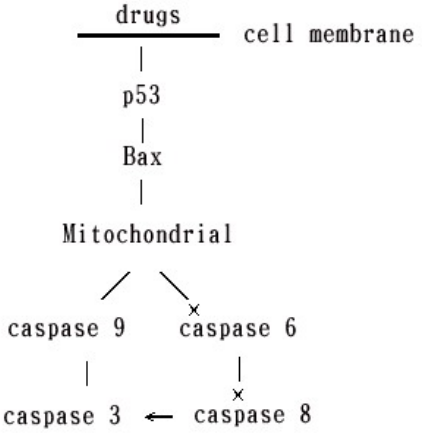

F**ig. 12b** The route of aloe-emodin metabolites on apoptosis pathway of NMDA-treated N18 RGCs. The apoptosis pathway of aloe-emodin metabolites and NMDA- cotreated N18 RGCs. NMDA and aloe-emodin metabolites acted in the apoptosis pathway by changing the expressions of p53, bax and caspase 9.

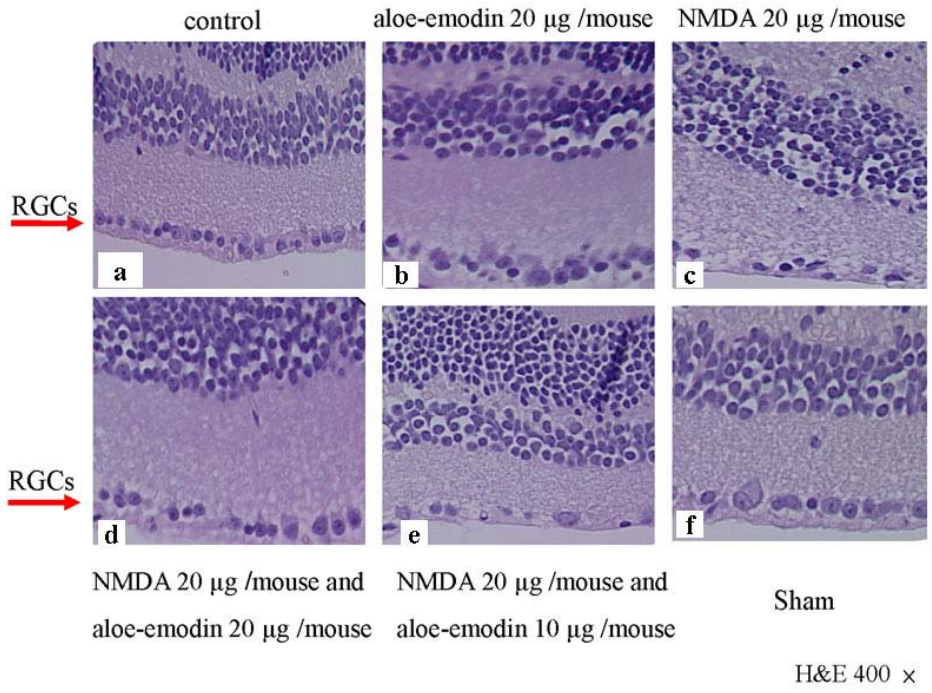

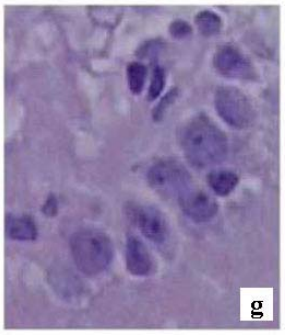

20 μg NMDA H&E 1600 X

Fig. 13 a-g Histologic examination of retina after NMDA and aloe-emodin were deliverd.

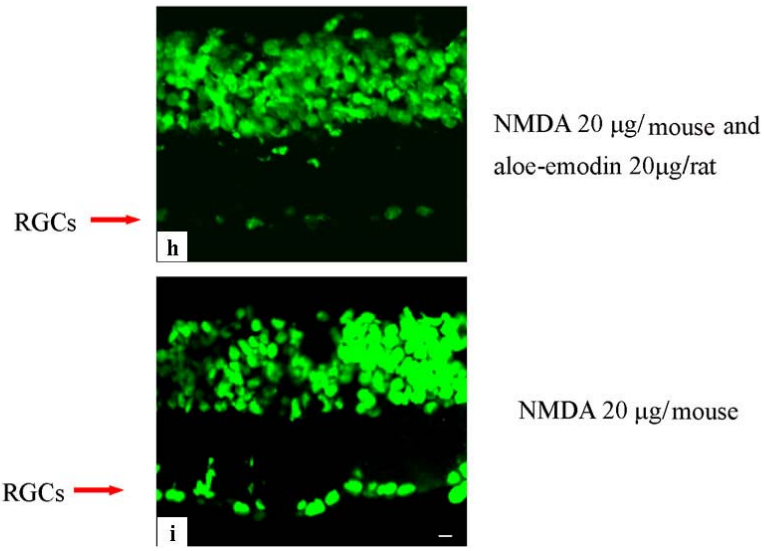

Fig. 13h and i TUNEL stain of retina after NMDA and aloe-emodin were deliverd.

Fig. 13 Histologic examination of retina after NMDA and aloe-emodin were deliverd. **Fig. 13a-g** RGCs were arranged in order at the inner layer of retina (Fig. 13a). Aloe-emodin (20 μg) itself was not toxic to RGCs (Fig. 13b). NMDA (20 μg) induced cell loss and apoptosis in RGCs (Fig. 13c, 13h); the nucleus of RGCs became irregular and fragmented. (Fig. 13g) Aloe-emodin (20 μg) increased the numbers and improved the arrangement of RGCs treated by NMDA (20 μg). (Fig. 13d, 13h) Aloe-emodin (40 μg) neither raised the numbers nor changed the appearances of NMDA (20 μg)-treated RGCs (Fig. 13e). When PEG 400 (40 μl) was delivered via deep sub-tendon injection; no evident change was noted (Fig. 13f). (Fig. 13a to Fig. 13f H&E 400× and Fig. 13g H&E 1600×). **Fig. 13h and i** TUNEL stain of retina after NMDA and aloe-emodin were deliverd. TUNEL positive RGCs were less in aloe-emodin 20 μg added RGCs then no aloe-emodin added RGCs. (In Fig. 13h and 13i, Scale bar = 1 μm) (ONL: outer nuclear layer, INL: inner nuclear layer. GCL: ganglion cell layer).

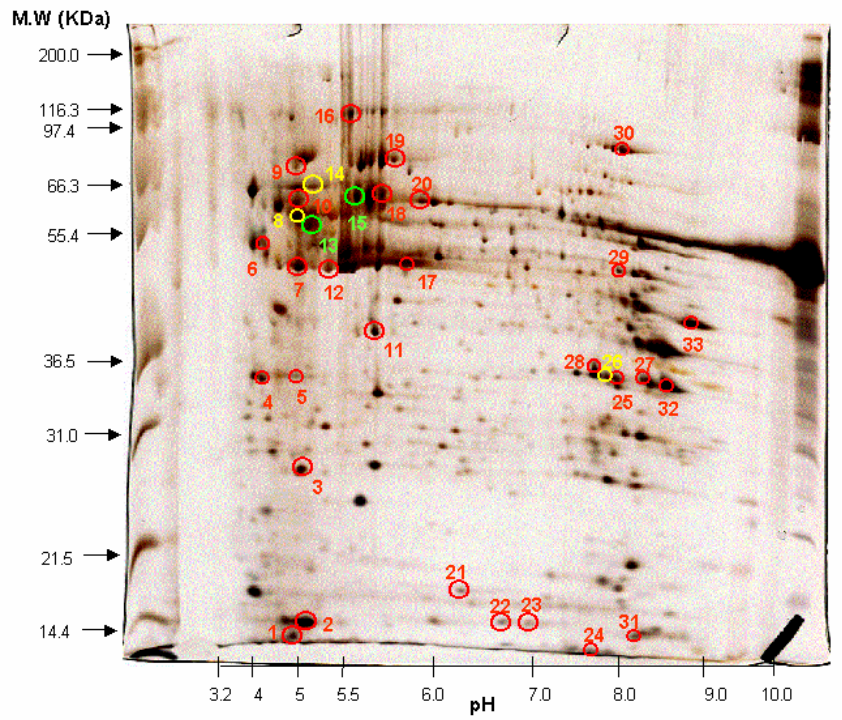

Fig. 14 Proteins expressed after N18 RGCs was co- treated with aloe-emodin metabolites and NMDA were selected from 2DE gel. Spots 1-33 existed only aloe-emodin was added to the cells and did not exist in negative control or only NMDA is added to the cells.

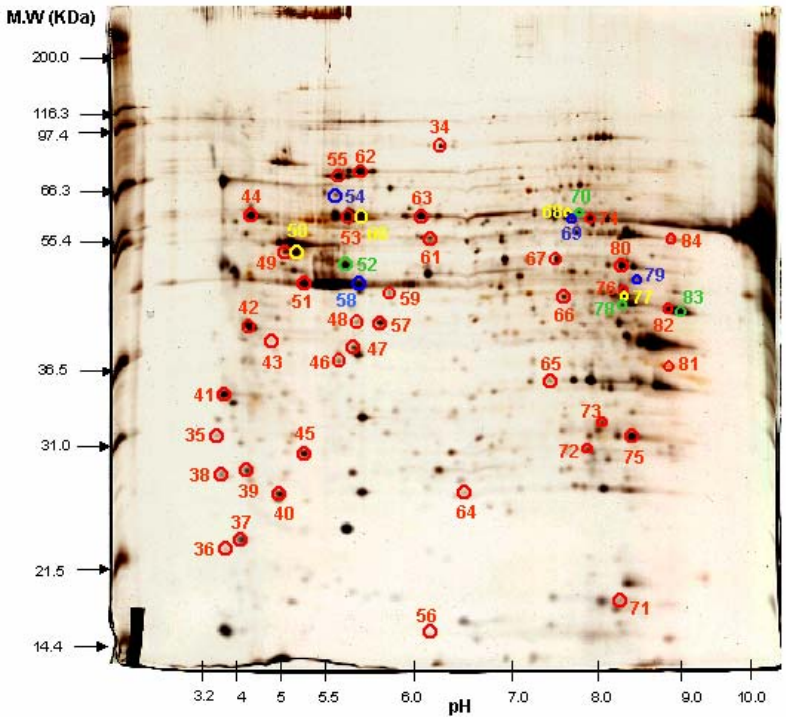

Fig. 15 Proteins preserved after aloe-emodin metabolites and NMDA-cotreated were selected from the 2DE gel of negative control. Spots 34- 84 existed in negative control and after aloe-emodin being added to the NMDA-treated cells but did not exist in the cells only treated with NMDA.

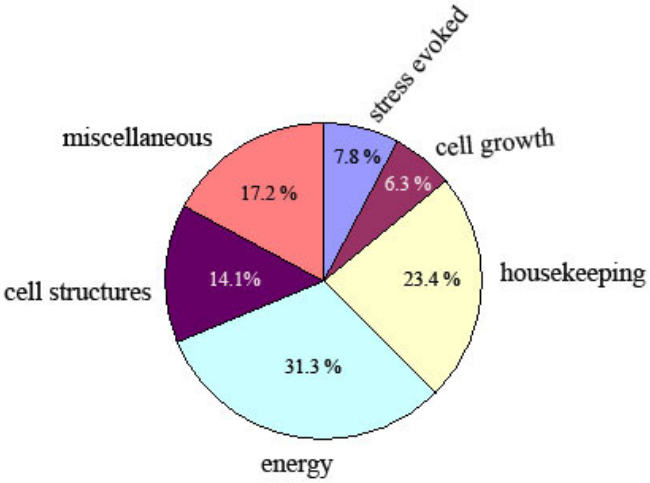

Fig. 16 The distribution of involved proteins in aloe-emodin and NMDA treated N18 RGCs. 1. Stress evoked proteins; 2. Proteins involved in cell growth; 3. Housekeeping proteins; 4. Proteins involved in production of energy in cells; 5. Proteins involved in formation of cells structure; 6. Miscellaneous proteins.

Fig. 17 (A)-(I) Identification of galectin-1, EF 1-β, Hsp60, stress-70 protein, Cu-Zn SOD, Hsp10, VDAC-1 Mitofilin, and PDI A6 precursor

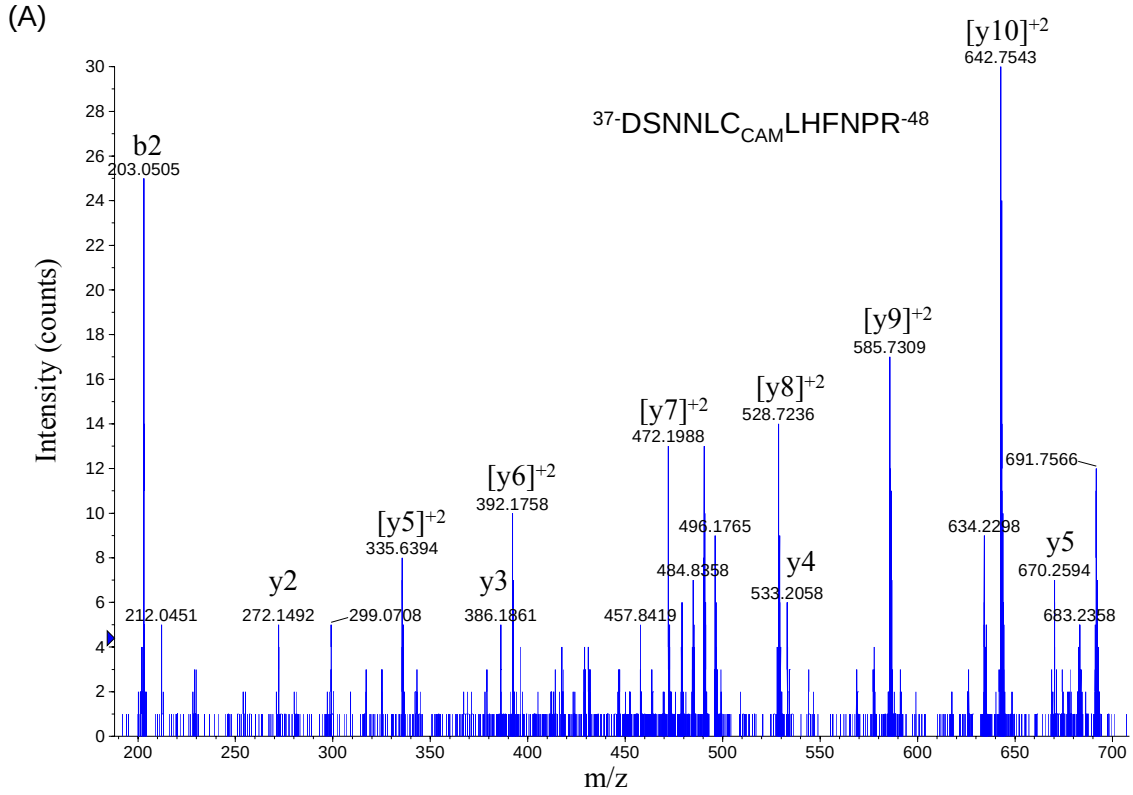

Fig. 17 (A) The nanoelectrospray mass spectrum of galectin-1

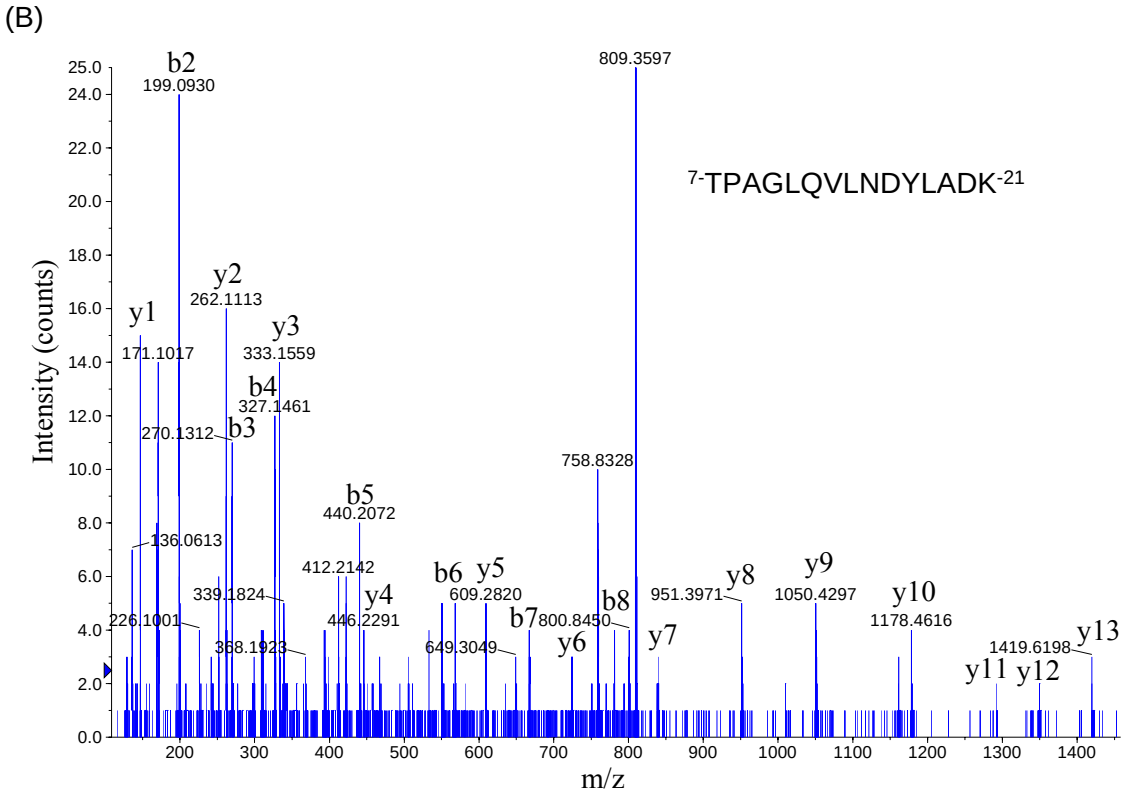

Fig. 17 (B) The nanoelectrospray mass spectrum of EF 1-β

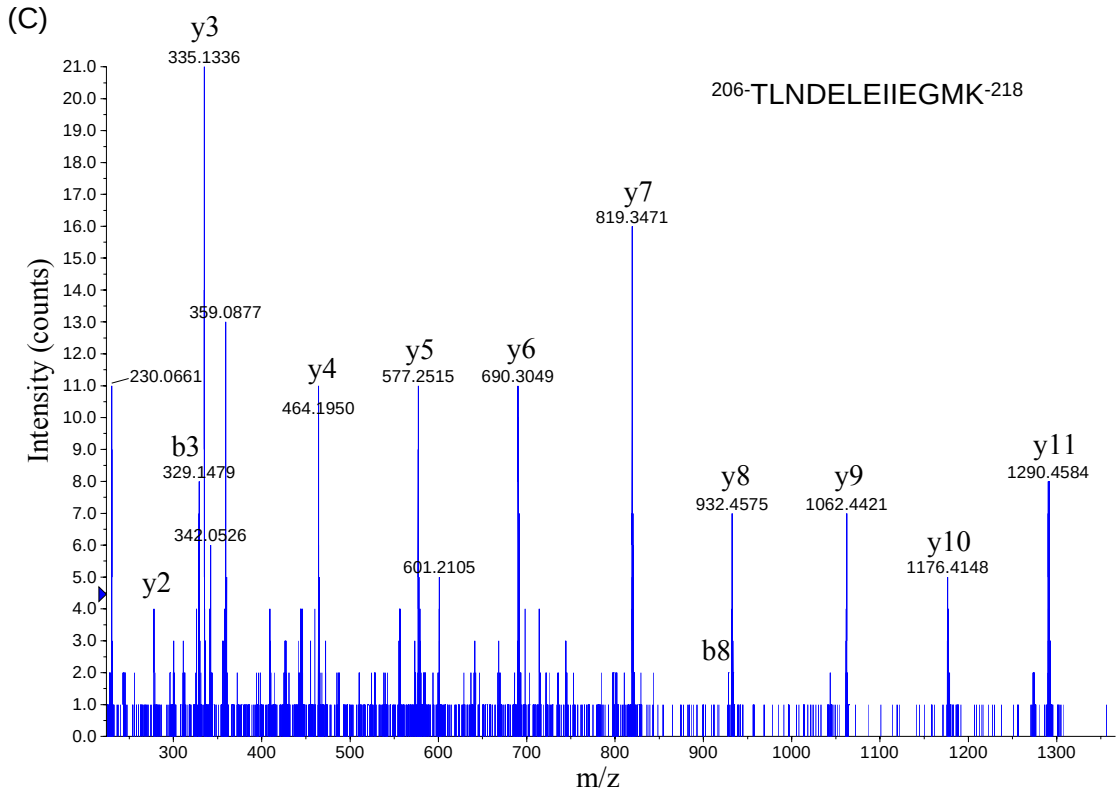

Fig. 17 (C) The nanoelectrospray mass spectrum of Hsp60

(D)

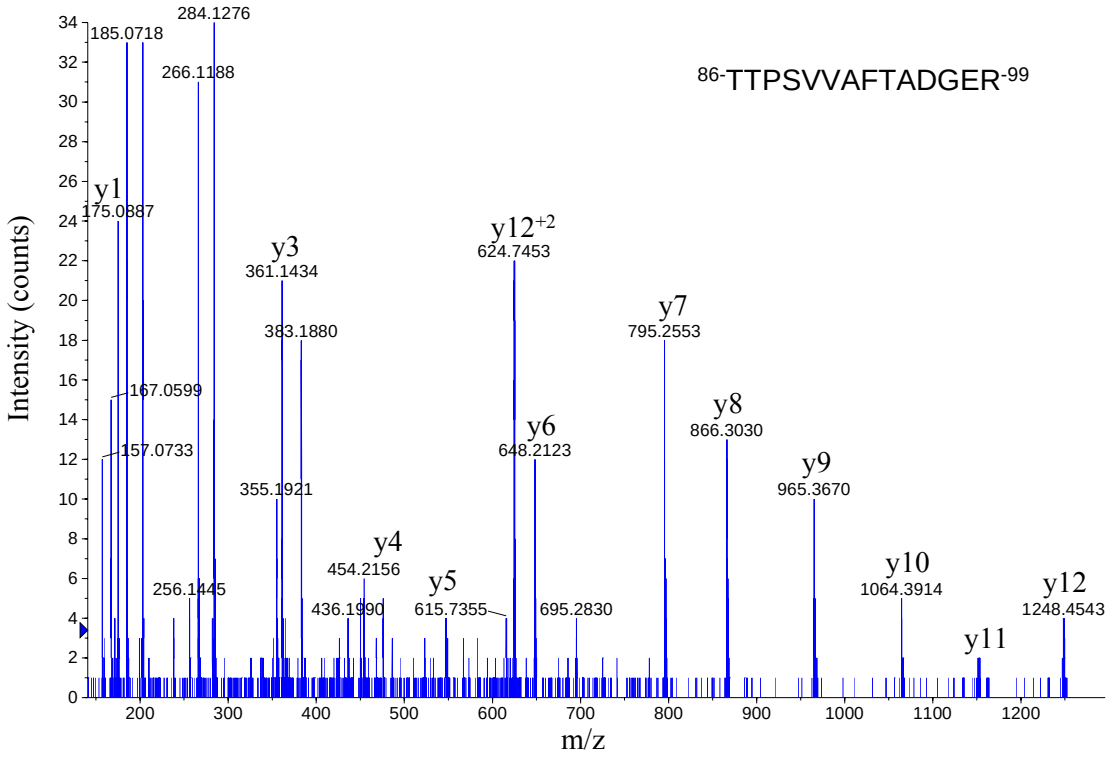

Fig. 17 (D) The nanoelectrospray mass spectrum of stress-70 protein

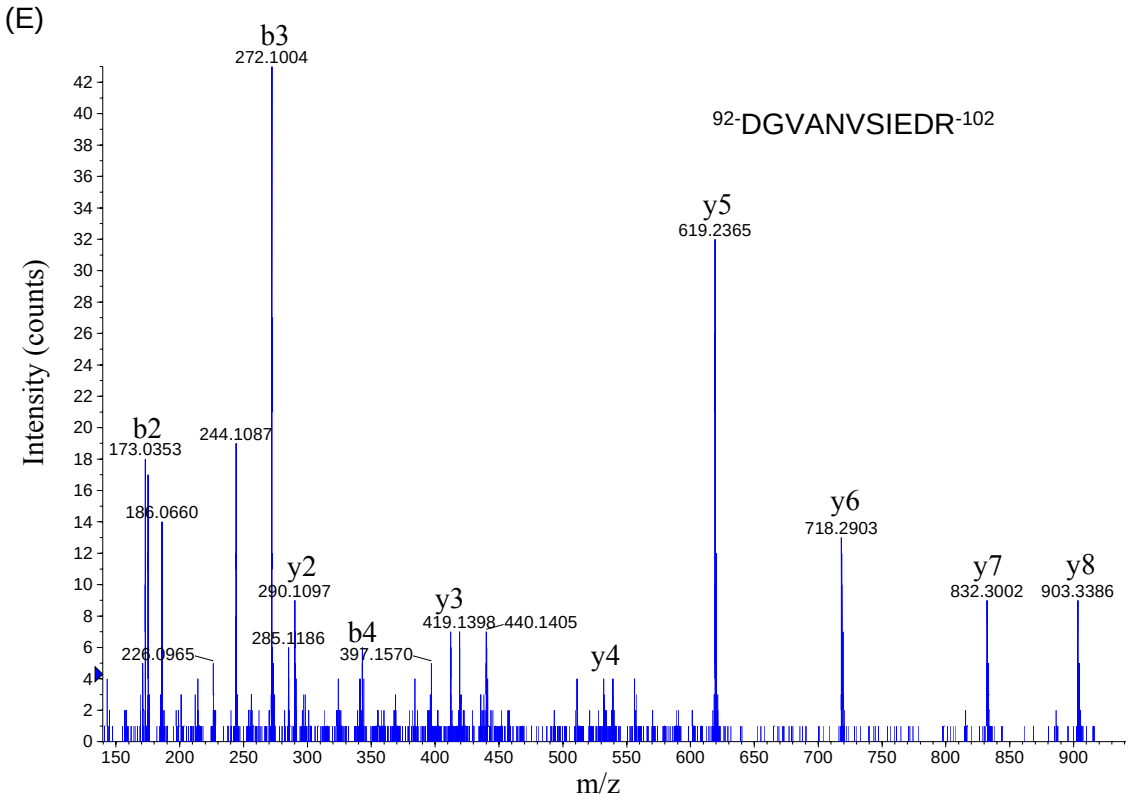

Fig. 17 (E) The nanoelectrospray mass spectrum of Cu-Zn SOD

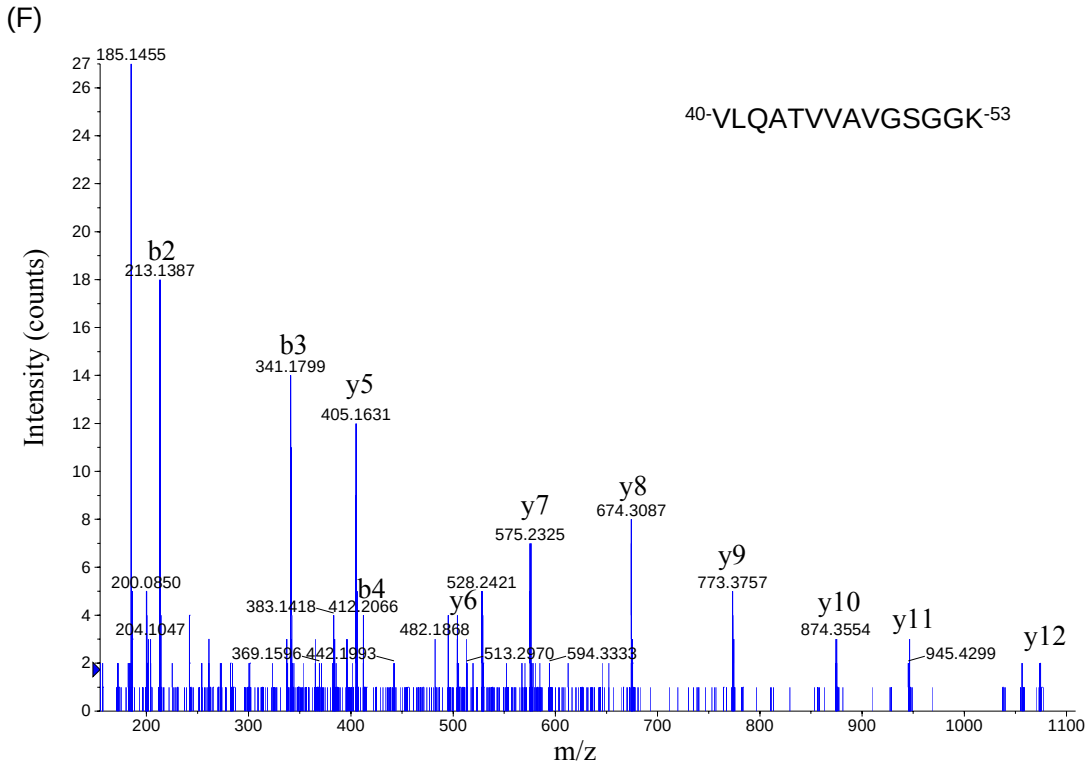

Fig. 17 (F) The nanoelectrospray mass spectrum of Hsp10

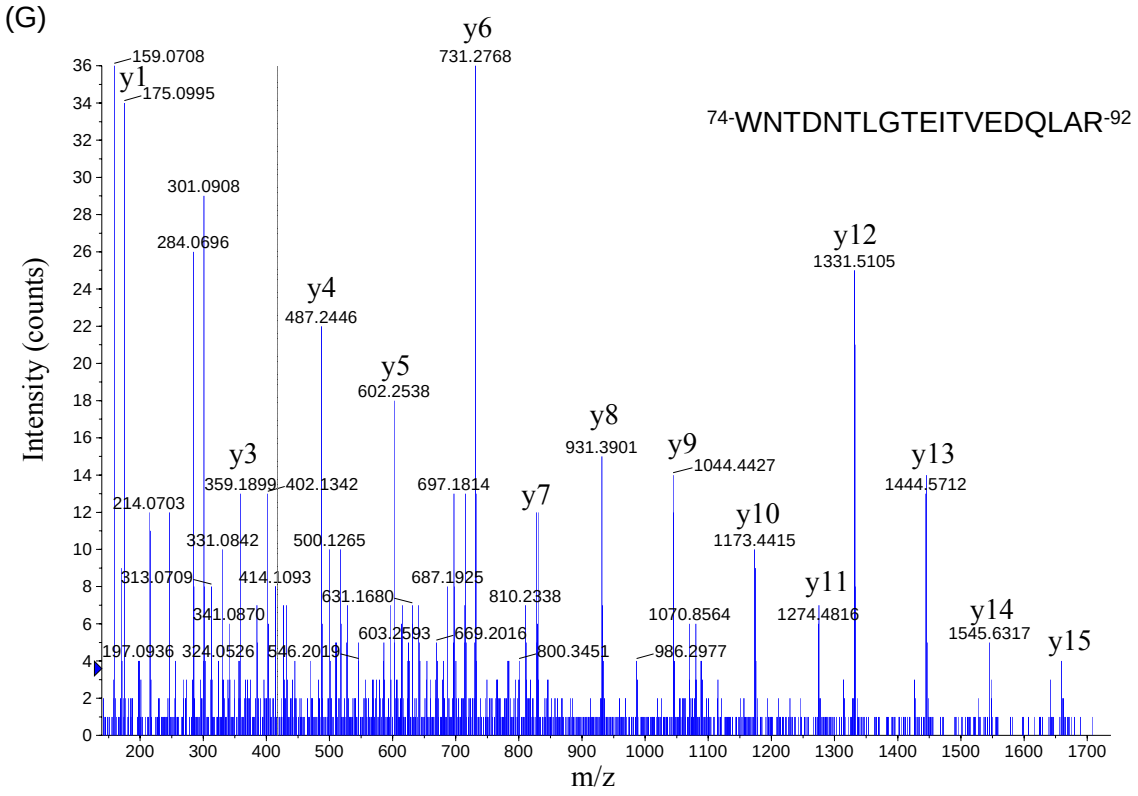

Fig. 17 (G) The nanoelectrospray mass spectrum VDAC-1

(H)

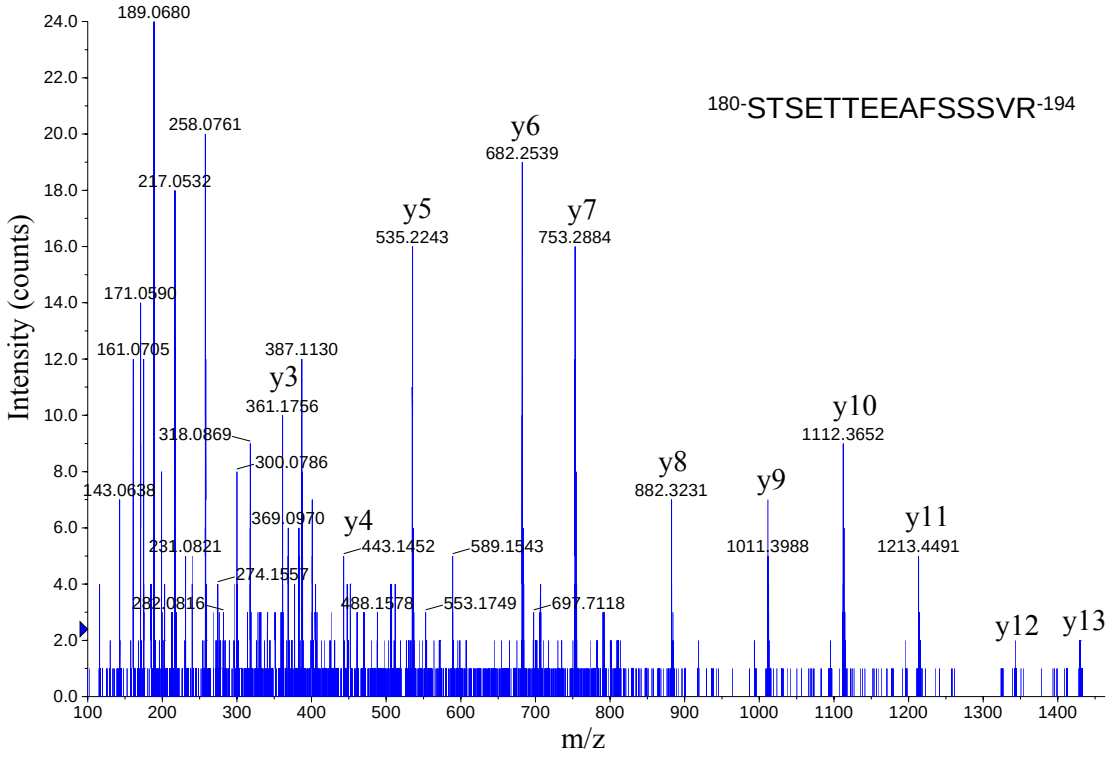

Fig. 17 (H) The nanoelectrospray mass spectrum mitofilin

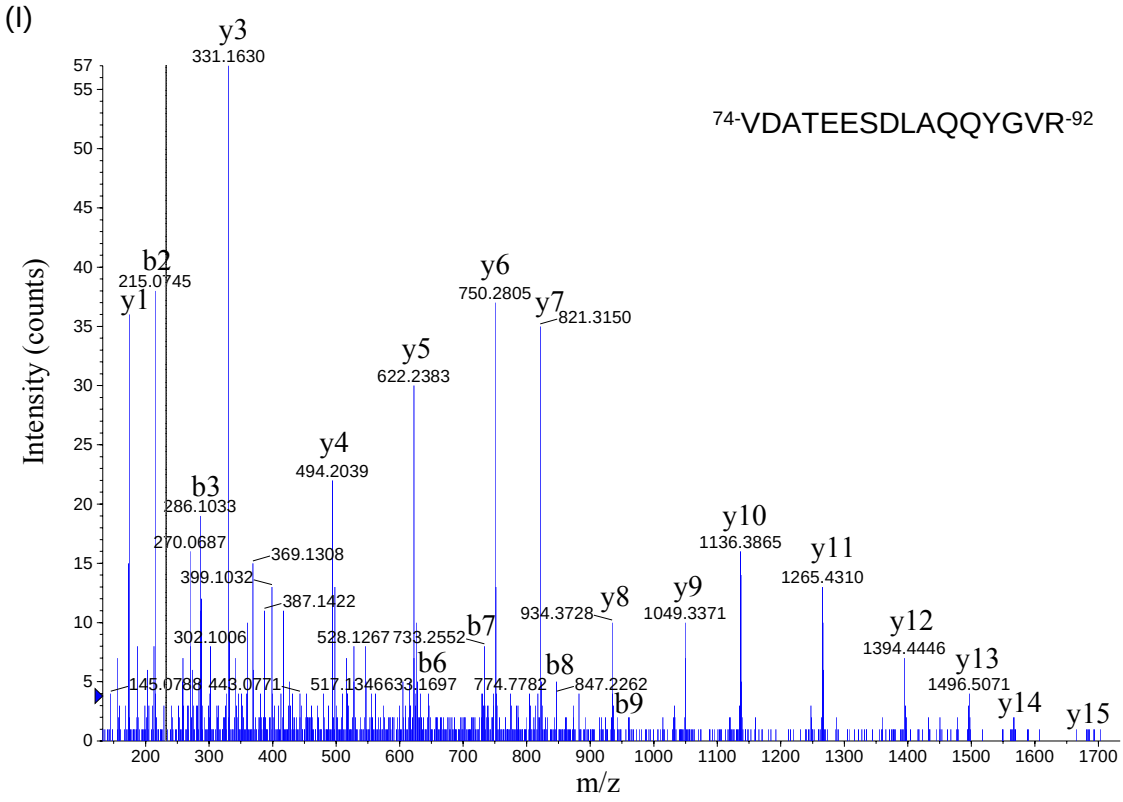

Fig. 17 (I) The nanoelectrospray mass spectrum of PDI A6 precursor

Fig. 17 Identification of galectin-1, EF 1-β, Hsp60, stress-70 protein, Cu-Zn SOD, Hsp10, VDAC-1, Mitofilin, and PDI A6 precursor (A) The nanoelectrospray mass spectrum of the triply charged ion m/z 496.22 for spot 2 is shown. The amino acid sequence DSNNLCLHFNPR was determined from mass differences in the y-fragment ions series and matched residues 37-48 of the mouse galectin-1. (B) The nanoelectrospray mass spectrum of the doubly charged ion m/z 809.42 for spot 4 is shown. The amino acid sequence TPAGLQVLNDYLADK was determined from mass differences in the y-fragment ions series and matched residues 7-21 of the mouse EF 1-β. (C) The nanoelectrospray mass spectrum of the doubly charged ion m/z 752.87 for spot 15 is shown. The amino acid sequence TLNDELEIIEGMK was determined from mass differences in the y-fragment ions series and matched residues 206-218 of the mouseHsp60. (D) The nanoelectrospray mass spectrum of the doubly charged ion m/z 725.83 for spot 19 is shown. The amino acid sequence TTPSVVAFTADGER was determined from mass differences in the y-fragment ions series and matched residues 86-99 of the stress-70 protein. (E) The nanoelectrospray mass spectrum of the doubly charged ion m/z 587.76 for spot 21 is shown. The amino acid sequence DGVANVSIEDR was determined from mass differences in the y-fragment ions series and matched residues 92-102 of the Cu-Zn SOD. (F) The nanoelectrospray mass spectrum of the doubly charged ion m/z 643.35 for spot 24 is shown. The amino acid sequence VLQATVVAVGSGGK was determined from mass differences in the y-fragment ions series and matched residues 40-53 of the Hsp 10. (G) The nanoelectrospray mass spectrum of the doubly charged ion m/z 1088.47 for spot 32 is shown. The amino acid sequence WNTDNTLGTEITVEDQLAR was determined from mass differences in the y-fragment ions series and matched residues 74-92 of the

VDAC-1. (H) The nanoelectrospray mass spectrum of the doubly charged ion m/z 809.31 for spot 34 is shown. The amino acid sequence STSETTEEAFSSSVR was determined from mass differences in the y-fragment ions series and matched residues 180-194 of the Mitofilin. (I) The nanoelectrospray mass spectrum of the doubly charged ion m/z 890.85 for spot 44 is shown. The amino acid sequence VDATEESDLAQQYGVR was determined from mass differences in the y-fragment ions series and matched residues 84-99 of the PDI A6 precursor.

*Only y- and b-fragment ions are labeled in the spectrum.

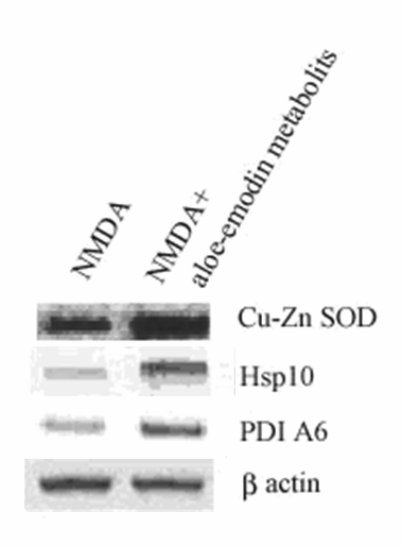

Fig. 18a Western blotting of Cu-Zn SOD, Hsp 10 and PDI A6 after aloe-emodin metabolites was added. Western blotting expressed of Cu-Zn SOD, Hsp10 and PDI A6 were up-regulated after aloe- emodin metabolites added to NMDA treated RGCs. The expression of Cu-Zn SOD had the most significant difference after aloe-emodin added to N18 RGCs.

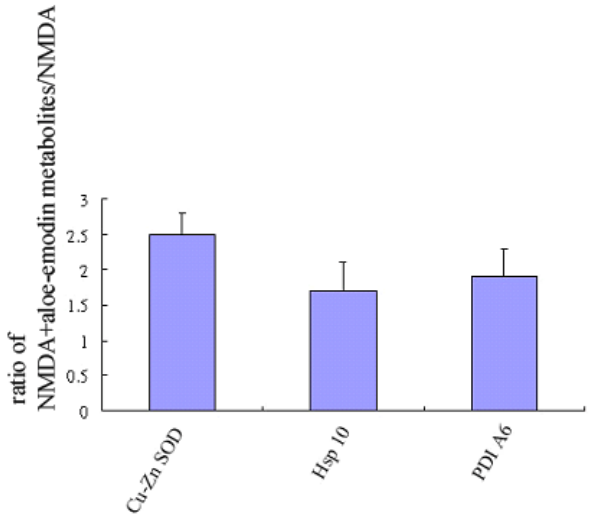

Fig. 18b The results of Western blotting after aloe-emodin metabolites was added. The expression of Cu-Zn SOD had the most significant difference after aloe-emodin added to N18 RGCs (p<0.05).